Radial-basis-function Calculations of Buoyancy-driven Flow in Concentric and Eccentric Annuli

K. Le-Cao, N. Mai-Duy and T. Tran-Cong

Computational Engineering and Science Research Centre
University of Southern Queensland, Queensland, 4350 AUSTRALIA

Abstract

This paper is concerned with the application of integrated radial-basis-function networks (IRBFNs) for the simulation of natural convection in concentric and eccentric annuli. Important features of the present technique include: (i) Taking a stream function - temperature formulation as the governing equations; (ii) Employing a Cartesian grid to discretize the problem domain; (iii) Using one-dimensional RBF approximations to represent the approximate solution; and (iv) Constructing the approximations through integration. These features result in an efficient numerical scheme as (i) the number of the governing differential equations is reduced from 4 to 2, (ii) the preprocessing is simple, (iii) the associated matrices have condition numbers in 2-norm that are much lower than those yielded through conventional RBF techniques, and (iv) the reduction of convergence rate caused by differentiation is avoided. A wide range of the Rayleigh number is considered. Results obtained are compared well with available numerical data in literature.
Keywords: Natural convection; Cartesian grid method; Irregular domain; Integrated radial basis function networks

Introduction

Natural convection is an important phenomenon in many applications in engineering and science such as meteorology, nuclear reactors and solar energy systems. The problem has thus been extensively studied by both experimental and theoretical approaches. The motion of a fluid is caused by the combination of density variations and gravity. Natural convection is governed by the coupling of momentum equation (velocity field) and energy equation (temperature field). Numerical solutions can be achieved by means of discretisation, followed by solutions of the resultant algebraic equations. Results have been reported using different discretisation techniques such as finite-difference methods (FDMs) (e.g. [1,10]), finite-element methods (FEMs) (e.g. [17,22]), finite-volume methods (FVMs) (e.g. [4,6]), boundary-element methods (BEMs) (e.g. [5,9,20]) and spectral methods (e.g. [11,24]).

RBFNs have been proved to be a universal approximator. Over the last fifteen years, the networks have been developed to solve different types of differential problems encountered in applied mathematics, science and engineering (e.g. [3,7,8,13,23,27]). RBFN methods are truly meshless, extremely easy to implement and capable of achieving a high level of accuracy using relatively small numbers of nodes. However, the RBF system matrix is fully populated and its condition number grows rapidly as the number of nodes is increased. One way to overcome these problems is to approximate the solution locally. Recently, one-dimensional (1D) IRBFN approximation schemes have been proposed in [16]. The "local" 1D-IRBFN approximations at a grid node involve only nodal points that lie on the grid lines intersected at that point rather than the whole set of nodes. Moreover, the construction of the RBF approximations is based on integration, which avoids the reduction of convergence rate caused by differentiation. Numerical results have indicated that this approach allows larger numbers of nodes to

be employed and is able to maintain a fast rate of convergence with grid refinement.

In this paper, we present the 1D-IRBFN technique for the simulation of buoyancy-driven flow governed by nonlinear partial differential equations (PDEs) and defined in concentric and eccentric annuli. For conventional FDMs and pseudospectral techniques, coordinate transformations are required to convert non-rectangular domains into rectangular ones [18,26]. The relationships between the physical and computational coordinates are given by a set of algebraic equations or a set of PDEs, depending on the level of complexity of the geometry. Such transformation processes are, in general, complicated. By contrast, the present method is able to retain the PDEs in their Cartesian forms, and thus work in a similar fashion for different shapes of annuli. In addition, the formulation of stream function and temperature is employed, which reduces the number of dependent variables from four (two velocity components, pressure and temperature) to two (stream function and temperature). An outline of the paper is as follows. First, a brief review of the governing equations is given. Then, the present 1D-IRBFN technique is described, followed by numerical results for natural convection in circular-circular and square-circular annuli. Finally, some remarks conclude the paper.

Governing Equations

Using the Boussinesq approximation, the 2D dimensionless forms of the PDEs governing buoyancy-driven flows can be written as (e.g. [19])

$$\frac{\partial u}{\partial x} + \frac{\partial v}{\partial y} = 0, \tag{1}$$

$$\frac{\partial u}{\partial t} + u\frac{\partial u}{\partial x} + v\frac{\partial u}{\partial y} = -\frac{\partial p}{\partial x} + \sqrt{\frac{Pr}{Ra}}\left(\frac{\partial^2 u}{\partial x^2} + \frac{\partial^2 u}{\partial y^2}\right), \tag{2}$$

$$\frac{\partial v}{\partial t} + u\frac{\partial v}{\partial x} + v\frac{\partial v}{\partial y} = -\frac{\partial p}{\partial y} + \sqrt{\frac{Pr}{Ra}}\left(\frac{\partial^2 v}{\partial x^2} + \frac{\partial^2 v}{\partial y^2}\right) + T, \tag{3}$$

$$\frac{\partial T}{\partial t} + u\frac{\partial T}{\partial x} + v\frac{\partial T}{\partial y} = \frac{1}{\sqrt{RaPr}}\left(\frac{\partial^2 T}{\partial x^2} + \frac{\partial^2 T}{\partial y^2}\right), \tag{4}$$

where u and v are the velocity components, p the dynamic pressure, T the temperature, and Pr and Ra the Prandtl and Rayleigh numbers defined as $Pr = \nu/\alpha$ and $Ra = \beta g\Delta T L^3/\alpha\nu$, respectively in which ν is the kinematic viscosity, α the thermal diffusivity, β the thermal expansion coefficient, g the gravity, and L and ΔT the characteristic length and temperature difference, respectively. In this dimensionless scheme, the velocity scale is taken as $U = \sqrt{gL\beta\Delta T}$ for the purpose of balancing the buoyancy and inertial forces.

By writing the velocity components in terms of a stream function ψ defined as

$$u = \frac{\partial\psi}{\partial y}, \quad v = -\frac{\partial\psi}{\partial x},$$

the continuity equation is satisfied identically and the momen-

tum equations reduce to

$$\frac{\partial}{\partial t}\left(\frac{\partial^2\psi}{\partial x^2}+\frac{\partial^2\psi}{\partial y^2}\right)+\frac{\partial\psi}{\partial y}\left(\frac{\partial^3\psi}{\partial x^3}+\frac{\partial^3\psi}{\partial x\partial y^2}\right)-\frac{\partial\psi}{\partial x}\left(\frac{\partial^3\psi}{\partial x^2\partial y}+\frac{\partial^3\psi}{\partial y^3}\right)$$
$$=\sqrt{\frac{Pr}{Ra}}\left(\frac{\partial^4\psi}{\partial x^4}+2\frac{\partial^4\psi}{\partial x^2\partial y^2}+\frac{\partial^4\psi}{\partial y^4}\right)-\frac{\partial T}{\partial x}. \quad (5)$$

It can be seen that one can replace the system of four equations (1)-(4) by a set of two equations (4) and (5). The latter will be employed in the present work.

The Present 1D-IRBFN Technique

One-dimensional IRBFNs

It is known that RBFNs have the property of universal approximation. The RBFN allows the conversion of a function to be approximated from a low-dimensional space (e.g., 1D here) to a high-dimensional space in which the function is expressed as a linear combination of RBFs

$$f(x)=\sum_{i=1}^{m}w_ig_i(x), \quad (6)$$

where m is the number of RBFs, $\{g_i(x)\}_{i=1}^{m}$ the set of RBFs, and $\{w_i\}_{i=1}^{m}$ the set of weights to be found. The present technique implements the multiquadric (MQ) function whose form is

$$g_i(x)=\sqrt{(x-c_i)^2+a_i^2}, \quad (7)$$

where c_i and a_i are the centre and the width of the ith basis function.

In the traditional/direct approach, a function f is approximated by an RBFN, followed by successive differentiations to obtain approximate expressions for its derivatives. There is a reduction in convergence rate for derivative functions and this reduction is an increasing function of derivative order [12].

Mai-Duy and Tran-Cong [14,15] have proposed the use of integration to construct the RBF approximations. A derivative of f is decomposed into RBFs, and lower-order derivatives and the function itself are then obtained through integration

$$\frac{d^pf(x)}{dx^p}=\sum_{i=0}^{m}w_ig_i(x)=\sum_{i=0}^{m}w_iI_i^{(p)}(x), \quad (8)$$

$$\frac{d^{p-1}f(x)}{dx^{p-1}}=\sum_{k=0}^{m}w_iI_i^{(p-1)}(x)+c_1, \quad (9)$$

$$\frac{d^{p-2}f(x)}{dx^{p-2}}=\sum_{k=0}^{m}w_iI_i^{(p-2)}(x)+c_1x+c_2, \quad (10)$$

$$\cdots \quad \cdots \quad \cdots \quad \cdots \quad \cdots$$

$$\frac{df(x)}{dx}=\sum_{k=0}^{m}w_iI_i^{(1)}(x)+c_1\frac{x^{p-2}}{(p-2)!}+c_2\frac{x^{p-3}}{(p-3)!}+\cdots+$$
$$c_{p-2}x+c_{p-1}, \quad (11)$$

$$f(x)=\sum_{k=0}^{m}w_iI_i^{(0)}(x)+c_1\frac{x^{p-1}}{(p-1)!}+c_2\frac{x^{p-2}}{(p-2)!}+\cdots+$$
$$c_{p-1}x+c_p, \quad (12)$$

where $I_i^{(p-1)}(x)=\int I_i^{(p)}(x)dx,$ $I_i^{(p-2)}(x)=\int I_i^{(p-1)}(x)dx,\cdots,I_i^{(0)}(x)=\int I_i^{(1)}(x)dx,$ and $c_1,c_2,\cdots,c_p$ are the constants of integration. Numerical results have shown that the integral approach significantly improves the quality of the approximation of derivative functions over conventional

differential approaches. The IRBF approximation scheme is said to be of pth-order, denoted by IRBFN-p, if the pth-order derivative is taken as the staring point.
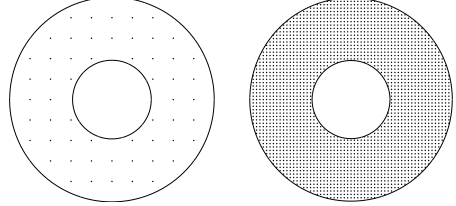
Simulation of Buoyancy-driven Flow

Figure 1: A circular-circular annulus: Computational domain and discretisations: 11×11 (left) and 61×61 (right).

Consider the process of natural convection between two cylinders, one heated and the other cooled (e.g. Figure 1). The problem domain is embedded in a Cartesian grid with a grid spacing h. Grid points outside the domain (external points) together with internal points that fall very close–within a distance of $h/8$–to the boundary are removed. The remaining grid points are taken to be the interior nodes. The boundary nodes consist of the grid points lying on the boundaries, and points generated by the intersection of the grid lines with the boundaries.

Along each grid line, 1D-IRBFNs are employed to approximate the solutions and their relevant derivatives. In what follows, the proposed method is described in detail for the energy equation (4) and the momentum equation (5). Special attention is given to the implementation of boundary conditions.

IRBFN Discretisation of The Energy Equation

The energy equation involves the following linear second-order differential operator

$$\mathcal{L}_2=\frac{\partial^2}{\partial x^2}+\frac{\partial^2}{\partial y^2}. \quad (13)$$

As presented earlier, an IRBFN-p scheme permits the approximation of a function and its derivatives of orders up to p. To use integrated basis functions only, one needs to employ IRBFNs of at least second order. A line in the grid contains two sets of points (Figure 2). The first set consists of the interior points that are also the grid nodes (regular nodes). The values of the temperature at the interior points are unknown. The second set is formed from the boundary nodes that do not generally coincide with the grid nodes (irregular nodes). At the boundary nodes, the values of the temperature are given.

For classical FDMs, the irregular nodes require changes of Δx and Δy in the finite-difference formulas, and such changes deteriorate the order of truncation error [22]. Unlike FD and also spectral approximation schemes, IRBFNs have the capability to handle unstructured points with high accuracy. As a result, the present technique does not require any special treatments for irregular boundary points. The boundary conditions are imposed through the process of converting the network-weight space into the physical space (conversion process).

Consider a horizontal grid line (Figure 2). An important feature of the present technique is that, along the grid line, both interior points $\{x_i\}_{i=1}^{q}$ and boundary points $\{x_{bi}\}_{i=1}^{2}$ are taken to be the centres of the network. We employ 1D-IRBFN-2s here to discretize the temperature field T. The conversion system is
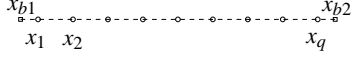
Figure 2: Points on a grid line consist of interior points x_i ($\circ$) and boundary points x_{bi} ($\square$).

constructed as follows

$$\left(\begin{array}{c} \widehat{T} \\ \widehat{T}_b \end{array} \right) = \widehat{\mathcal{C}} \, \widehat{w}, \tag{14}$$

where

$$\widehat{T} = \left(T_1, T_2, \cdots, T_q \right)^T,$$
$$\widehat{T}_b = \left(T_{b1}, T_{b2} \right)^T,$$
$$\widehat{w} = \left(w_1, w_2, \cdots, w_m, c_1, c_2 \right)^T,$$

$$\widehat{\mathcal{C}} = \left[\begin{array}{cccccc} I_1^{(0)}(x_1) & \cdots & I_m^{(0)}(x_1) & x_1 & 1 \\ I_1^{(0)}(x_2) & \cdots & I_m^{(0)}(x_2) & x_2 & 1 \\ \cdots & \cdots & \cdots & \cdots & \cdots \\ I_1^{(0)}(x_q) & \cdots & I_m^{(0)}(x_q) & x_q & 1 \\ I_1^{(0)}(x_{b1}) & \cdots & I_m^{(0)}(x_{b1}) & x_{b1} & 1 \\ I_1^{(0)}(x_{b2}) & \cdots & I_m^{(0)}(x_{b2}) & x_{b2} & 1 \end{array} \right],$$

and $m = q + 2$.

The obtained system (14) for the unknown vector of network weights can be solved using the singular value decomposition technique

$$\widehat{w} = \widehat{\mathcal{C}}^{-1} \left(\begin{array}{c} \widehat{T} \\ \widehat{T}_b \end{array} \right). \tag{15}$$

Taking (15) into account, the values of the first and second derivatives of T at the interior points are computed by

$$\left(\begin{array}{c} \frac{\partial T_1}{\partial x} \\ \frac{\partial T_2}{\partial x} \\ \vdots \\ \frac{\partial T_q}{\partial x} \end{array} \right) = \widehat{I}_{[2]}^{(1)} \widehat{\mathcal{C}}^{-1} \left(\begin{array}{c} \widehat{T} \\ \widehat{T}_b \end{array} \right), \tag{16}$$

and

$$\left(\begin{array}{c} \frac{\partial^2 T_1}{\partial x^2} \\ \frac{\partial^2 T_2}{\partial x^2} \\ \vdots \\ \frac{\partial^2 T_q}{\partial x^2} \end{array} \right) = \widehat{I}_{[2]}^{(2)} \widehat{\mathcal{C}}^{-1} \left(\begin{array}{c} \widehat{T} \\ \widehat{T}_b \end{array} \right), \tag{17}$$

where

$$\widehat{I}_{[2]}^{(1)} = \left[\begin{array}{ccccc} I_1^{(1)}(x_1) & \cdots & I_m^{(1)}(x_1) & 1 & 0 \\ I_1^{(1)}(x_2) & \cdots & I_m^{(1)}(x_2) & 1 & 0 \\ \cdots & \cdots & \cdots & \cdots & \cdots \\ I_1^{(1)}(x_q) & \cdots & I_m^{(1)}(x_q) & 1 & 0 \end{array} \right],$$

and

$$\widehat{I}_{[2]}^{(2)} = \left[\begin{array}{ccccc} I_1^{(2)}(x_1) & \cdots & I_m^{(2)}(x_1) & 0 & 0 \\ I_1^{(2)}(x_2) & \cdots & I_m^{(2)}(x_2) & 0 & 0 \\ \cdots & \cdots & \cdots & \cdots & \cdots \\ I_1^{(2)}(x_q) & \cdots & I_m^{(2)}(x_q) & 0 & 0 \end{array} \right].$$

Expressions (16) and (17) can be rewritten in compact forms

$$\widehat{\frac{\partial T}{\partial x}} = \widehat{\mathcal{D}}_{1x} \widehat{T} + \widehat{k}_{1x}, \tag{18}$$

and

$$\widehat{\frac{\partial^2 T}{\partial x^2}} = \widehat{\mathcal{D}}_{2x} \widehat{T} + \widehat{k}_{2x}, \tag{19}$$

where $\widehat{k}_{1x}$ and $\widehat{k}_{2x}$ are the vectors of known quantities related to boundary conditions.

It can be seen from (18) and (19) that the IRBFN approximations of $\partial T / \partial x$ and $\partial^2 T / \partial x^2$ at the interior points include information about the inner and outer boundaries (locations and boundary values). Thus it remains only to force these approximations to satisfy the governing equation.

The incorporation of the boundary points into the set of centres has several advantages:

- It allows the two sets of centres and collocation points to be the same, i.e. $\{c_i\}_{i=1}^m \equiv \left\{ \{x_i\}_{i=1}^q \cup \{x_{bi}\}_{i=1}^2 \right\}$. Numerical investigations [16,23] have indicated that, when these two sets coincide, the RBF approximation scheme tends to result in the most accurate approximate solution.

- It allows the use of IRBFNs with a fixed order (IRBFN-2), regardless of the shape of the domain.

In the same manner, one can obtain the IRBF expressions for $\partial T / \partial y$ and $\partial^2 T / \partial y^2$ at the interior points along a vertical line.

As with FDMs, FVMs, BEMs and FEMs, the IRBF approximations will be gathered together to form the global matrices for the discretisation of the PDE. By collocating the governing equation at the interior points, a square system of algebraic equations is obtained, which is solved for the approximate temperature at the interior points.

IRBFN Discretisation of The Momentum Equation

The momentum equation involves the following linear fourth-order differential operator

$$\mathcal{L}_4 = \frac{\partial^4}{\partial x^4} + 2 \frac{\partial^4}{\partial x^2 \partial y^2} + \frac{\partial^4}{\partial y^4}. \tag{20}$$

At each boundary node, the solution is required to satisfy two prescribed values, ψ and $\partial \psi / \partial n$. It is straightforward to obtain the values of $\partial \psi / \partial x$ and $\partial \psi / \partial y$ at the boundary nodes from the prescribed conditions. The double boundary conditions are implemented through the conversion process of the network-weight space into the physical space.

Along each grid line, the set of centres also consists of the interior points and the boundary points. The addition of extra equations to the conversion system for the purpose of representing derivative boundary conditions is offset by the generation of additional unknowns of the integral collocation approach. Consider a horizontal grid line (Figure 2). The present work employs 1D-IRBFN-4s to approximate the variable ψ. The conversion system is given by

$$\left(\begin{array}{c} \widehat{\psi} \\ \widehat{\psi}_b \\ \frac{\partial \widehat{\psi}_b}{\partial x} \end{array} \right) = \widehat{\mathcal{C}} \, \widehat{w}, \tag{21}$$

where

$$\widehat{\psi} = \left(\psi_1, \psi_2, \cdots, \psi_q \right)^T,$$
$$\widehat{\psi}_b = \left(\psi_{b1}, \psi_{b2} \right)^T,$$
$$\frac{\partial \widehat{\psi}_b}{\partial x} = \left(\frac{\partial \psi_{b1}}{\partial x}, \frac{\partial \psi_{b2}}{\partial x} \right)^T,$$
$$\widehat{w} = \left(w_1, w_2, \cdots, w_m, c_1, c_2, c_3, c_4 \right)^T,$$

$$\widehat{C} = \begin{bmatrix} I_1^{(0)}(x_1) & \cdots & I_m^{(0)}(x_1) & x_1^3/6 & x_1^2/2 & x_1 & 1 \\ I_1^{(0)}(x_2) & \cdots & I_m^{(0)}(x_2) & x_2^3/6 & x_2^2/2 & x_2 & 1 \\ \cdots & \cdots & \cdots & \cdots & \cdots & & \\ I_1^{(0)}(x_q) & \cdots & I_m^{(0)}(x_q) & x_q^3/6 & x_q^2/2 & x_q & 1 \\ I_1^{(0)}(x_{b1}) & \cdots & I_m^{(0)}(x_{b1}) & x_{b1}^3/6 & x_{b1}^2/2 & x_{b1} & 1 \\ I_1^{(0)}(x_{b2}) & \cdots & I_m^{(0)}(x_{b2}) & x_{b2}^3/6 & x_{b2}^2/2 & x_{b2} & 1 \\ I_1^{(1)}(x_{b1}) & \cdots & I_m^{(1)}(x_{b1}) & x_{b1}^2/2 & x_{b1} & 1 & 0 \\ I_1^{(1)}(x_{b2}) & \cdots & I_m^{(1)}(x_{b2}) & x_{b2}^2/2 & x_{b2} & 1 & 0 \end{bmatrix},$$

and $m = q + 2$. The values of the lth-order derivative ($l = \{1,2,3,4\}$) of ψ at the interior points on the line are evaluated as

$$\widehat{\frac{\partial^4 \psi}{\partial x^4}} = \widehat{I}_{[4]}^{(4)} \widehat{C}^{-1} \begin{pmatrix} \widehat{\psi} \\ \widehat{\psi}_b \\ \frac{\partial \psi_b}{\partial x} \end{pmatrix}, \tag{22}$$

$$\widehat{\frac{\partial^3 \psi}{\partial x^3}} = \widehat{I}_{[4]}^{(3)} \widehat{C}^{-1} \begin{pmatrix} \widehat{\psi} \\ \widehat{\psi}_b \\ \frac{\partial \psi_b}{\partial x} \end{pmatrix}, \tag{23}$$

$$\widehat{\frac{\partial^2 \psi}{\partial x^2}} = \widehat{I}_{[4]}^{(2)} \widehat{C}^{-1} \begin{pmatrix} \widehat{\psi} \\ \widehat{\psi}_b \\ \frac{\partial \psi_b}{\partial x} \end{pmatrix}, \tag{24}$$

and

$$\widehat{\frac{\partial^1 \psi}{\partial x^1}} = \widehat{I}_{[4]}^{(1)} \widehat{C}^{-1} \begin{pmatrix} \widehat{\psi} \\ \widehat{\psi}_b \\ \frac{\partial \psi_b}{\partial x} \end{pmatrix}, \tag{25}$$

where

$$\widehat{I}_{[4]}^{(4)} = \begin{bmatrix} I_1^{(4)}(x_1) \cdots I_m^{(4)}(x_1) & 0 & 0 & 0 & 0 \\ I_1^{(4)}(x_2) \cdots I_m^{(4)}(x_2) & 0 & 0 & 0 & 0 \\ \cdots & \cdots & \cdots & \cdots & \cdots \\ I_1^{(4)}(x_q) \cdots I_m^{(4)}(x_q) & 0 & 0 & 0 & 0 \end{bmatrix},$$

$$\widehat{I}_{[4]}^{(3)} = \begin{bmatrix} I_1^{(3)}(x_1) \cdots I_m^{(3)}(x_1) & 1 & 0 & 0 & 0 \\ I_1^{(3)}(x_2) \cdots I_m^{(3)}(x_2) & 1 & 0 & 0 & 0 \\ \cdots & \cdots & \cdots & \cdots & \cdots \\ I_1^{(3)}(x_q) \cdots I_m^{(3)}(x_q) & 1 & 0 & 0 & 0 \end{bmatrix},$$

$$\widehat{I}_{[4]}^{(2)} = \begin{bmatrix} I_1^{(2)}(x_1) \cdots I_m^{(2)}(x_1) & x_1 & 1 & 0 & 0 \\ I_1^{(2)}(x_2) \cdots I_m^{(2)}(x_2) & x_2 & 1 & 0 & 0 \\ \cdots & \cdots & \cdots & \cdots & \cdots \\ I_1^{(2)}(x_q) \cdots I_m^{(2)}(x_q) & x_q & 1 & 0 & 0 \end{bmatrix},$$

and

$$\widehat{I}_{[4]}^{(1)} = \begin{bmatrix} I_1^{(1)}(x_1) \cdots I_m^{(1)}(x_1) & x_1^2/2 & x_1 & 1 & 0 \\ I_1^{(1)}(x_2) \cdots I_m^{(1)}(x_2) & x_2^2/2 & x_2 & 1 & 0 \\ \cdots & \cdots & \cdots & \cdots & \cdots \\ I_1^{(1)}(x_q) \cdots I_m^{(1)}(x_q) & x_q^2/2 & x_q & 1 & 0 \end{bmatrix}.$$

Expressions (22)-(25) can reduce to

$$\widehat{\frac{\partial^l \psi}{\partial x^l}} = \widehat{\mathcal{D}}_{lx} \widehat{\psi} + \widehat{k}_{lx}, \tag{26}$$

where $\widehat{k}_{lx}$ are the vectors of known quantities related to boundary conditions. Since the discretisation used has a structured form, the process of joining "local" 1D-IRBF approximations together (assemblage process) is quite straightforward. For a special case of rectangular domain, the IRBF approximations over a 2D domain can simply be constructed using the tensor direct product.

The fourth- and also third-order mixed derivatives are computed using the following relations

$$\frac{\partial^4 \psi}{\partial^2 x \partial^2 y} = \frac{1}{2} \left[\frac{\partial^2}{\partial x^2} \left(\frac{\partial^2 \psi}{\partial y^2} \right) + \frac{\partial^2}{\partial y^2} \left(\frac{\partial^2 \psi}{\partial x^2} \right) \right], \tag{27}$$

$$\frac{\partial^3 \psi}{\partial^2 x \partial y} = \frac{\partial^2}{\partial x^2} \left(\frac{\partial \psi}{\partial y} \right), \tag{28}$$

$$\frac{\partial^3 \psi}{\partial x \partial y^2} = \frac{\partial^2}{\partial y^2} \left(\frac{\partial \psi}{\partial x} \right). \tag{29}$$

Expressions (27)-(29) reduce the computation of mixed derivatives to that of lower-order pure derivatives for which IRBFNs involve integration with respect to x or y only. The additional work here is the computation of $\partial^2(F)/\partial x^2$ and $\partial^2(F)/\partial y^2$ where F is a derivative function of ψ (i.e. $\partial^2 \psi/\partial y^2, \partial^2 \psi/\partial x^2, \partial \psi/\partial y$ and $\partial \psi/\partial x$). It can be seen that the discretisation of (5) requires the values of the mixed derivatives at the interior points. IRBFN-2s can be employed here to construct the approximations for $\partial^2(F)/\partial x^2$ and $\partial^2(F)/\partial y^2$. Both sets of centres and collocation points of these second-order networks consist of the interior nodes only. The IRBF expressions for derivatives are now written in terms of the values of ψ at the interior points, and they already satisfy the boundary conditions. These nodal variable values are determined by forcing the approximate solution to satisfy the momentum equation at the interior points. Like the energy equation, the resultant system of algebraic equations here is of size $n_{ip} \times n_{ip}$, where n_{ip} is the number of interior points of the domain.

Solution Procedure

The energy and momentum equations must be solved simultaneously to find the values of the temperature and stream function at discrete points within the domain. Because of the presence of convective terms in the governing equations, the obtained algebraic equations for the discrete solution are nonlinear. In this paper, a time dependent decoupled approach is employed to handle this nonlinearity. The advantage of this approach is that it allows the breakdown of the problem into the solution of the energy equation and the solution of the momentum equation (two smaller subproblems at each iteration).

The nonlinear equation set is solved in a marching manner.

1. Guess initial values of T, ψ and their first-order spatial derivatives at time $t = 0$.

2. Discretize the governing equations in time using a first-order accurate finite-difference scheme, where the diffusive and convective terms are treated implicitly and explicitly, respectively.

3. Discretize the governing equations in space using 1D-IRBF schemes:
   Solve the energy equation (4) for T, and
   Solve the momentum equation (5) for ψ.
   The two equations are solved separately in order to keep matrix sizes to a minimum.

4. Check to see whether the solution has reached a steady state

$$CM = \frac{\sqrt{\sum_{i=1}^{n_{ip}} \left(\psi_i^{(k)} - \psi_i^{(k-1)} \right)^2}}{\sqrt{\sum_{i=1}^{n_{ip}} \left(\psi_i^{(k)} \right)^2}} < \varepsilon, \tag{30}$$

where k is the time level and ε is the tolerance.

5. If it is not satisfied, advance time step and repeat from step 2. Otherwise, stop the computation and output the results.

Numerical Results

The present method is applied to the simulation of buoyancy-driven flow in concentric and eccentric annuli. A wide range of the Rayleigh number is considered. The computed solution at the lower and nearest value of Ra is taken to be the initial solution. The MQ-RBF width is simply chosen to be the grid size h.

Natural Convection in A Circular Annulus

Consider the natural convection between two concentric cylinders which are separated by a distance L, the inner cylinder heated and the outer cylinder cooled (Figure 1). A comprehensive review of this problem can be found in [10]. Most cases have been reported with $Pr = 0.7$ and $L/D_i = 0.8$, in which D_i is the diameter of the inner cylinder. These conditions are also employed in the present work. Kuehn and Goldstein [10] have also reported numerical results by FDM for $Ra = 10^2$ to $Ra = 7 \times 10^4$. Using the differential quadrature method (DQM), Shu [24] has provided very accurate solutions for values of the Rayleigh number in the range of 10^2 to 5×10^4.

One typical quantity associated with this type of flow is the average equivalent conductivity denoted by $\bar{k}_{eq}$. This quantity is defined as ([10,24])

$$\bar{k}_{eq} = \frac{-\ln(D_o/D_i)}{2\pi} \oint \frac{\partial T}{\partial n} ds \qquad (31)$$
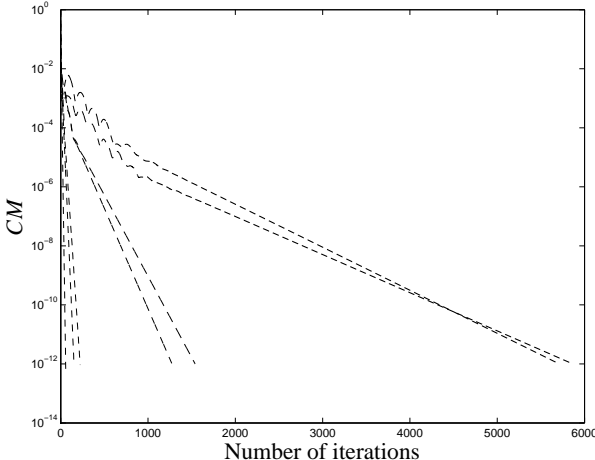
in which D_o is the diameter of the outer cylinder.

Figure 3: Iterative convergence. Time steps used are 0.5 for $Ra = \{10^2, 10^3, 3 \times 10^3\}$, 0.1 for $Ra = \{6 \times 10^3, 10^4\}$, and 0.05 for $Ra = \{5 \times 10^4, 7 \times 10^4\}$. The values of CM become less than 10^{-12} when the numbers of iterations reach 58, 154, 224, 1276, 1541, 5711 and 5867 for $Ra = \{10^2, 10^3, 3 \times 10^3, 6 \times 10^3, 10^4, 5 \times 10^4, 7 \times 10^4\}$, respectively.

The stream function and its normal derivative are set to zero along the inner and outer cylinders. The temperature is held at $T = 1$ at the inner cylinder and $T = 0$ at the outer cylinder. We employ a number of uniform Cartesian grids, namely $11 \times 11, 21 \times 21, \cdots, 61 \times 61$, to study the behaviour of grid convergence of the present method. The convergence of the iterative procedure with respect to time step is shown in Figure 3.
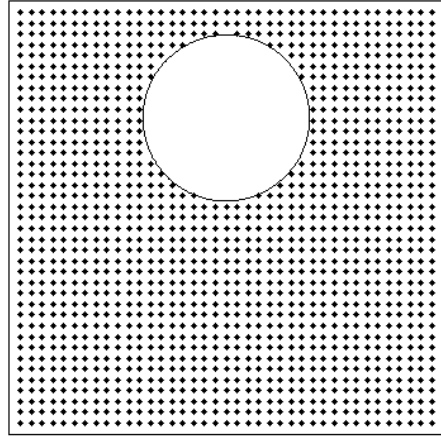

Figure 4: An eccentric square-circular annulus: Computational domain and discretisation

The condition numbers of matrices associated with harmonic (13) and biharmonic (20) operators in the governing equations (4) and (5) are reported in Table 1.

Grid	cond($\mathcal{L}_2 T$)	cond($\mathcal{L}_4 \psi$)
11×11	1.3×10^1	7.4×10^1
21×21	1.2×10^2	5.0×10^3
31×31	3.3×10^2	3.3×10^4
41×41	5.1×10^2	7.9×10^4
51×51	7.5×10^2	1.6×10^5
61×61	1.0×10^3	3.2×10^5

Table 1: Circular cylinders: Condition numbers of matrices associated with harmonic and biharmonic operators.

Results concerning $\bar{k}_{eq}$ together with those of Kuehn and Goldstein [10] and of Shu [24] for $Ra = \{10^3, 6 \times 10^3, 5 \times 10^4, 7 \times 10^4\}$ are presented in Tables 2-5. It can be seen that there is a good agreement between these numerical solutions. For each Rayleigh number, the convergence of the average equivalent conductivity with grid refinement is fast.

Also, we consider eccentric circular-circular annuli, where the centre of an inner cylinder lies on the vertical symmetrical axis of an outer cylinder. Different amounts of eccentricity (e), namely $-0.95, -0.75, -0.5, -0.25, 0.25, 0.5, 0.75$ and 0.95, are employed. Since the flow is symmetric, the stream function on the outer and inner cylinders have the same value and they can be set to zeros. Results concerning ψ_{max} together with those of Shu and Zhu [25] for $Ra = 10^4$ are presented in Table 6. It can be seen that both numerical results are in good agreement. Figure 5 shows the streamlines and isotherms of the flow for $Ra = 10^4$ using a grid of 41×41. Each plot contains 21 contour lines whose levels vary linearly from the minimum to maximum values. The plots look reasonable when compared with those of the DQM method.

Grid	Outer cylinder, k_{eqo}	Inner cylinder, k_{eqi}
11×11	1.133	1.046
21×21	1.072	1.069
31×31	1.078	1.077
41×41	1.080	1.079
51×51	1.081	1.080
FDM [10]	1.084	1.081
DQM [24]	1.082	1.082

Table 2: Circular cylinders: Convergence of computed average equivalent conductivities with grid refinement for $Ra = 10^3$.

Grid	Outer cylinder, k_{eqo}	Inner cylinder, k_{eqi}
31×31	1.698	1.702
41×41	1.704	1.705
51×51	1.709	1.709
61×61	1.711	1.711
FDM [10]	1.735	1.736
DQM [24]	1.715	1.715

Table 3: Circular cylinders: Convergence of computed average equivalent conductivities with grid refinement for $Ra = 6 \times 10^3$.

Grid	Outer cylinder, k_{eqo}	Inner cylinder, k_{eqi}
41×41	3.089	3.045
51×51	2.936	2.946
61×61	2.922	2.941
FDM [10]	2.973	3.024
DQM [24]	2.958	2.958

Table 4: Circular cylinders: Convergence of computed average equivalent conductivities with grid refinement for $Ra = 5 \times 10^4$.

Grid	Outer cylinder, k_{eqo}	Inner cylinder, k_{eqi}
41×41	3.465	3.254
51×51	3.241	3.187
61×61	3.167	3.174
FDM [10]	3.226	3.308

Table 5: Circular cylinders: Convergence of computed average equivalent conductivities with grid refinement for $Ra = 7 \times 10^4$.

e	ψ_{max}	
	Present	DQM[25]
-0.95	22.193	22.162
-0.75	20.721	20.627
-0.5	18.504	18.325
-0.25	15.719	15.508
+0.25	11.269	11.138
+0.5	9.648	9.556
+0.75	8.255	8.127
+0.95	7.284	7.172

Table 6: Eccentric circular-circular annuli: Comparison of ψ_{max} for $Ra = 10^4$ between the present technique and DQM.

e	ψ_{max}	
	Present	MQ-DQ[2]
-0.75	23.56	23.52
-0.25	18.68	18.64
+0.25	12.40	12.39
+0.75	10.10	10.09

Table 7: Eccentric square-circular annuli: Comparison of ψ_{max} for $Ra = 3 \times 10^5$ between the present technique and DQM.

Natural Convection in Eccentric Square-Circular Annuli

Consider the natural convection between a heated inner circular cylinder and a cooled square enclosure with their centres lying on the vertical line (Figure 4). An aspect ratio of $L/2R = 0.26$ (L: the side length of the outer square and R: the radius of the inner circle), $Pr = 0.71$, $Ra = \{5 \times 10^4, 3 \times 10^5, 7 \times 10^5, 10^6\}$ and $e = \{-0.75, -0.25, 0.25, 0.75\}$ are considered. Like the previous problem, the values of ψ along the inner and outer boundaries can be taken to be zeros. Calculations are conducted on a uniform Cartesian grid of 41×41.

Values of ψ_{max} are given in Table 7. It can be seen that the present results agree well with those of Ding and Shu [2]. Other results, namely streamlines and isotherms, are shown in Figure 6, where each plot contains 21 contour lines with their levels varying linearly from the minimum to maximum values.

Concluding Remarks

In this article, we present a numerical scheme based on Cartesian grids and 1D-IRBFNs for the simulation of natural convection in circular-circular and square-circular annuli. The main advantages of the present technique lie in the simplicity of the preprocessing, the ease of implementation and the achievement of high Rayleigh-number solutions. Accurate results are obtained using relatively coarse grids. This study further demonstrates the great potential of the RBF technique for solving complex fluid-flow problems. Extension of the present technique to the case of unsymmetric annuli is currently carried out, and it will be reported in future work.
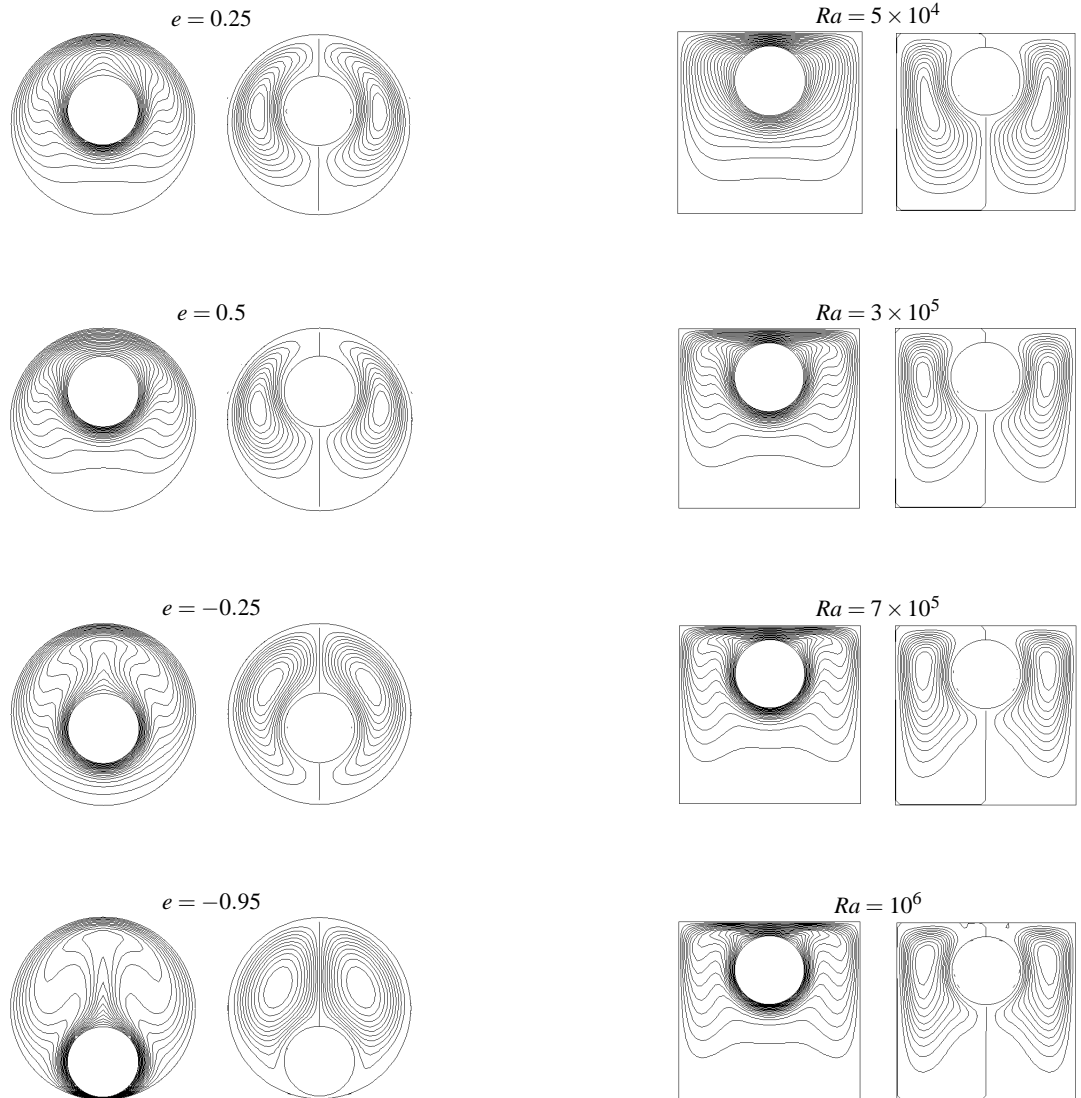
Acknowledgements

Figure 5: Eccentric circular-circular cylinders: Contour plots of temperature (left) and stream function (right) for the flow at $Ra = 10^4$ and four different values of e using a grid of 41×41.
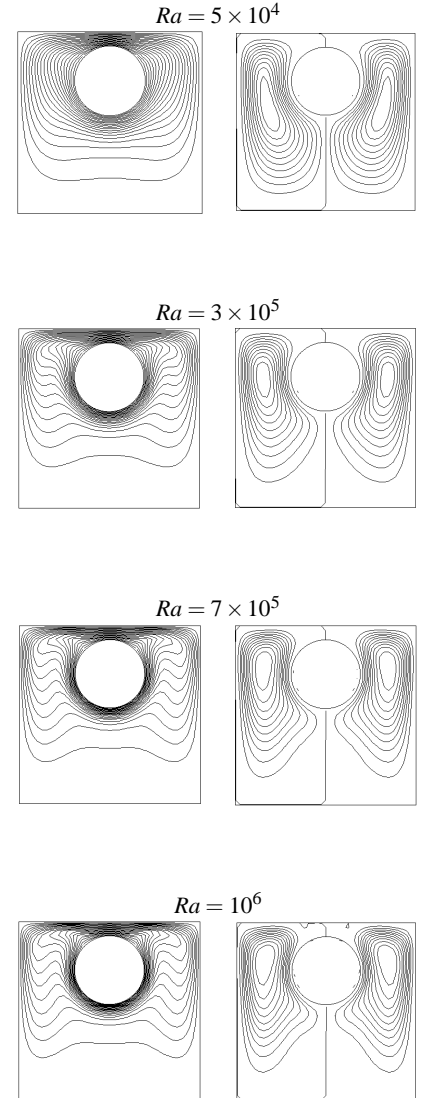

Figure 6: Eccentric square-circular cylinders: Contour plots of temperature (left) and stream function (right) for the flow at $e = 0.75$ and four different values of Ra using a grid of 41×41.

References

[1] de Vahl Davis, G., Natural convection of air in a square cavity: a bench mark numerical solution, *International Journal for Numerical Methods in Fluids*, **3**, 1983, 249–264.

[2] Ding, H. and Shu, C., Simulation of natural convection in eccentric annuli between a square outer cylinder and a circular inner cylinder using local MQ-DQ method, *International Journal of Computation and Methodology*, **47**, 2005, 271–313.

[3] Fasshauer, G.E., Solving partial differential equations by collocation with radial basis functions, in *Surface Fitting and Multiresolution Methods*, editors A. Le Mehaute, C. Rabut and L.L., Schumaker, Nashville, TN, Vanderbilt University Press, 1997, 131–138.

[4] Glakpe, E.K., Watkins, C.B. and Cannon, J.N., Constant heat flux solutions for natural convection between concentric and eccentric horizontal cylinders, *Numerical Heat Transfer*, **10**, 1986, 279–295.

[5] Hribersek, M. and Skerget, L., Fast boundary-domain integral algorithm for the computation of incompressible fluid flow problems, *International Journal for Numerical Methods in Fluids*, **31**, 1999, 891–907.

[6] Kaminski, D.A. and Prakash, C., Conjugate natural convection in a square enclosure: effect of conduction in one of the vertical walls, *International Journal for Heat and Mass Transfer*, **29**(12), 1986, 1979–1988.

[7] Kansa, E.J., Multiquadrics- A scattered data approximation scheme with applications to computational fluid-dynamics-II. Solutions to parabolic, hyperbolic and elliptic partial differential equations, *Computers and Mathematics with Applications*, **19**(8/9), 1990, 147–161.

[8] Kansa, E.J. and Hon, Y.C., Circumventing the ill-conditioning problem with multiquadric radial basis functions: applications to elliptic partial differential equations, *Computers and Mathematics with Applications*, **39**, 2000, 123–137.

[9] Kitagawa, K., Wrobel, L.C., Brebbia, C.A. and Tanaka, M., A boundary element formulation for natural convection problems, *International Journal for Numerical Methods in Fluids*, **8**, 1988, 139–149.

[10] Kuehn, T.H. and Goldstein, R.J., An experimental and theoretical study of natural convection in the annulus between horizontal concentric cylinders, *Journal of Fluid Mechanics*, **74**(4), 1976, 695–719.

[11] Le Quere, P., Accurate solutions to the square thermally driven cavity at high Rayleigh number, *Computers & Fluids*, **20**(1), 1991, 29–41.

[12] Madych, W.R. and Nelson, S.A., Multivariate interpolation and conditionally positive definite functions, II,*Mathematics of Computation*, **54**(189), 1990, 211–230.

[13] Mai-Duy, N. and Tran-Cong, T., Numerical solution of differential equations using multiquadric radial basis function networks, *Neural Networks*, **14**(2), 2001, 185–199.

[14] Mai-Duy, N. and Tran-Cong, T., Numerical solution of Navier-Stokes equations using multiquadric radial basis function networks,*International Journal for Numerical Methods in Fluids*, **37**, 2001, 65–86.

[15] Mai-Duy, N. and Tran-Cong, T., Approximation of function and its derivatives using radial basis function networks, *Applied Mathematical Modelling*, **27**, 2003, 197–220.

[16] Mai-Duy, N. and Tran-Cong, T., A Cartesian-grid collocation method based on radial-basis-function networks for solving PDEs in irregular domains, *Numerical Methods for Partial Differential Equations*,**23**(5), 2007, 1192–1210.

[17] Manzari, M.T., An explicit finite element algorithm for convection heat transfer problems, *International Journal of Numerical Methods for Heat and Fluid Flow*, **9**(8), 1999, 860–877.

[18] Moukalled, F. and Acharya, S., Natural convection in the annulus between concentric horizontal circular and square cylinders, *Journal of Thermophysics and Heat Transfer*, **10**(3), 1996, 524–531.

[19] Ostrach, S., Natural convection in enclosures, *Journal of Heat Transfer*, **110**, 1988, 1175–1190.

[20] Power, H. and Mingo, R., The DRM sub-domain decomposition approach for two-dimensional thermal convection flow problems, *Engineering Analysis with Boundary Elements*, **24**, 2000, 121–127.

[21] Roache, P.J., *Computational Fluid Dynamics*, Albuquerque, Hermosa Publishers, 1980.

[22] Sammouda, H., Belghith, A. and Surry, C., Finite element simulation of transient natural convection of low-Prandtl-number fluids in heated cavity, *International Journal of Numerical Methods for Heat and Fluid Flow*, **9**(5), 1999, 612–624.

[23] Sarler, B., A radial basis function collocation approach in computational fluid dynamics, *Computer Modeling in Engineering and Sciences*, **7**(2), 2005, 185–194.

[24] Shu, C., Application of differential quadrature method to simulate natural convection in a concentric annulus, *International Journal for Numerical Methods in Fluids*, **30**, 1999, 977–993.

[25] Shu, C. and Zhu, Y.D., Numerical analysis of flow and thermal field in arbitrary eccentric annulus by differential quadrature method, *Journal for Heat and Mass transfer*, **38**, 2001, 597–608.

[26] Shu, C. and Zhu, Y.D., Efficient computation of natural convection in a concentric annulus between an outer square cylinder and an inner circular cylinder, *International Journal for Numerical Methods in Fluids*, **38**, 2002, 429–445.

[27] Zerroukat, T., Power, H. and Chen, C.S., A numerical method for heat transfer problems using collocation and radial basis functions, *International Journal for Numerical Methods in Engineering*, **42**, 1998, 1263–1278.